JOURNAL OF MATERIALS SCIENCE **34** (1999) 257–265

Mechanically alloyed Ni/8YSZ powder mixtures: preparation, powder characterization and sintering behavior

R. WILKENHOENER, R. VAßEN, H. P. BUCHKREMER, D. STÖVER
Institut für Werkstoffe und Verfahren der Energietechnik (IWV1), Forschungszentrum Juelich GmbH, D-52425 Juelich, Germany
E-mail: r.vassen@fz-juelich.de

A state of the art anode for the solid oxide fuel cell (SOFC) consists of a mixture of 8 mol % Y_2O_3-stabilized zirconia (8YSZ) and nickel particles, which form an interconnected porous structure after sintering. Coarsening of the Ni particles under SOFC working conditions has to be avoided, hence it leads to a deterioration of the anode's performance. In the present work the aim was to improve the stability of the Ni particles by a reduction of the sintering activity of nickel. For this purpose between 10 and 50% by volume of nano-sized zirconia particles have been dispersed in the nickel matrix by dry ball milling in a planetary mill. For pressed samples made of mechanically alloyed Ni with 10 vol % of 8YSZ, a homogeneous dispersion of 8YSZ particles in the Ni matrix was confirmed by transmission electron microscopy. It was confirmed by mercury porosity penetration and optical microscopy that this dispersoid structure leads to a retardation of recrystallization. Also, an essentially lowered densification during sintering was found, compared to samples made of the pure Ni powder. Samples made of mechanically alloyed Ni with a higher zirconia amount showed a higher densification during sintering and annealing than samples containing 10 vol % 8YSZ. It is assumed that this results from insufficient dispersion in these systems. The results show that mechanically alloyed nickel, with a homogeneous dispersion of 8YSZ crystallites, is a promising candidate for high temperature catalysts.

1. Introduction

Solid oxide fuel cells (SOFCs) are electric power generators which directly convert the chemical energy of combustible gases (e.g. H_2, CO or CH_4) into electric energy. Unlike heat engines, SOFCs are not limited by Carnot's rule and are expected to achieve an energy efficiency of up to 60%. Therefore, and because of their low emission of pollutants, SOFCs are promising electric power generators for the future. A SOFC consists of two electrodes, e.g. the anode (nickel/zirconia cermet) and the cathode (perovskite on the base of $LaMnO_3$), separated by an electrolyte. The electrolyte is made of a material with a high oxygen ion conductivity at the SOFC working temperature of 800–1050 °C; nowadays the electrolyte is 8 mol % Y_2O_3-stabilized zirconia (8YSZ). The fuel is fed to the anode where it is oxidized and electrons are released to the external (outer) circuit. The oxidant (O_2 or air) is reduced at the cathode and electrons are taken up from the external circuit. This electron flow from the anode to the cathode produces direct-current electricity. The electrolyte conducts the oxygen ions from the cathode to the anode [1, 2].

Each component of the SOFC serves several functions and must meet certain requirements. The anode has to fulfill the following requirements: (i) electronic conductivity (ensured by a continuous Ni structure), (ii) anodic properties (realized by a fine distribution of Ni particles, especially at the interface with the electrolyte), (iii) long-term functionality, which includes chemical compatibility with the materials of the neighboring components and proper stability (chemical, phase, microstructural and dimensional) in oxidizing and/or reducing environments, (iv) similar coefficients of thermal expansion of interconnect and electrolyte, (v) high permeability for the fuel and the reaction products H_2O and CO_2. In addition to the above requirements, other desirable properties from a practical viewpoint are fabricability and low cost.

One of the major problems of the SOFC is the deterioration of its performance with time. The deterioration is caused by structural changes in the components or by chemical interactions between the component materials under SOFC working conditions. Degradation of the anode due to microstructural changes contributes substantially to such deterioration. A state of the art anode for the SOFC consists of a mixture of 8YSZ and Ni particles which have been connected by sintering to a continuous and porous structure. In former studies

it was shown that coarsening of the Ni particles occurs under SOFC working conditions, which leads to a deterioration of the anode's electrochemical performance [3]. The driving force for this sintering process is the reduction of the total surface energy of the Ni phase by particle coarsening.

The aim of the present work was to determine if nickel strengthened by 8YSZ dispersion leads to a decrease of nickel sintering under SOFC working conditions. Dispersion strengthening of metals and alloys (e.g. nickel-based superalloys for gas turbine applications) is a state of the art method for improving their high-temperature and creep strength [4]. There are several mechanisms known by which the dispersoid structure causes these improved high-temperature properties, such as bowing of dislocations (Orowan strengthening) and grain-size refinement during recrystallization for oxide dispersion strengthened (ODS) superalloys, as well as stabilizing a fine grain/subgrain structure for Al alloys [4]. It is also known that dispersions of particles in metal powders might effectively inhibit the sintering [5]. An overview of this phenomena is found in the paper of Ashby *et al*. [6]; details are given in the discussion.

Ni powder was mechanically alloyed with various amounts of 8YSZ in order to verify the hypothesis that also the sintering of nickel powder is inhibited by a dispersion of fine ceramic particles. The sintering behavior at various sintering temperatures as well as structural changes during an isothermal annealing at 1000 °C were investigated on samples produced by pressing these powders.

We also tried to directly produce the anode cermet powders by mechanical alloying. The idea was to manufacture a suitable anode substrate for an anode-supported SOFC cell by the following process steps: (i) high-energy milling of the powder mixture leading to a partial dispersion of 8YSZ in the Ni particles, (ii) pressing of the green anode substrate using the milled powder, (iii) a final sintering process.

2. Experimental procedure

Nickel powder from Merck, Germany (No. 12277, purity >99.5%, particle size 6.4 μm) and (8YSZ) powder from Tosoh Corporation (JP, TZ-8Y) were used as starting materials. The 8YSZ powder appears as spherical agglomerates with diameters ranging from 5 to 50 μm. On a smaller scale, it exhibits particles of about 0.3 μm with a rather homogeneous morphology, which consist of crystallites with a size of less than 30 nm. The Ni powder was mechanically alloyed with 10, 25 and 50 vol % 8YSZ powder by dry milling the powder mixtures in a planetary mill (PM-4, Retsch, Germany). Zirconia containers and zirconia media balls were employed in order to ensure that no material other than zirconia could contaminate the Ni powder. Each container was filled with 100 g of powder. A large media diameter of 10 mm and a high media-to-powder ratio of 6 : 1 by weight were chosen to ensure high-energy milling.

TABLE I Batches of produced powder mixtures and milling parameters

Batch	Composition (vol %)	Rotation speed during milling (r.p.m.)	Milling time (h)
MA1	Ni	150	90
MA2	Ni + 10% 8YSZ	150	90
MA3	Ni + 25% 8YSZ	150	90
MA4	Ni + 50% 8YSZ	150	90
MA5	Ni + 25% 8YSZ	250	90

Milling was performed in air. This practice actually promotes mechanical alloying by particle welding in contrast to conventional metal ball milling practices in which welding is inhibited by the use of liquids and surfacants.

The various batches of produced powder are given in Table I. Pure Ni powder was milled in the first batch to provide a reference point for determining how the 8YSZ proportion influences the change in Ni particle size during milling. In addition, the amounts of zirconium and oxygen in this batch were measured after milling. From the results it can be deduced that each powder batch contains approximately 4 wt % of zirconia wear and 4 wt % of NiO after 90 h of milling.

Unfortunately, a complete dispersion of the high 8YSZ proportion of 50 vol % in batch MA4 in the Ni particles was not possible.

Milling was performed continuously except for batch MA5. For this batch a higher container rotation speed of 250 revolutions per minute (r.p.m.) was used. To avoid excessive warming of the powder, the milling process had to be stopped every two hours for one hour.

The particle size of the powder batches after various milling times was determined by using a laser light diffraction granulometer (Analysette 22, Fritsch, Germany). Their phase composition was measured by X-ray diffraction (Siemens D5000, Siemens, Germany). The plastic deformation of the Ni particles during milling leads to a grain refinement and a lattice distortion, whereby these effects may be intensified by dispersion of 8YSZ crystallites in the Ni. Both effects cause a broadening of the diffraction peaks with milling time. If a sufficiently high number of suitable peaks for a powder can be analyzed, a calculation of the mean crystallite size and the apparent lattice distortion from the half-peak widths by linear regression as described in [7] is possible. The results depend on the expression used to describe the peak line shape (e.g. Cauchy or Gauss) and on the correction of the measured half-peak width. In this study the calculations were performed using both expressions for the line shape and by correcting the measured half-peak width by (i) a constant half-peak width of 0.13 ° pertaining to the apparatus or (ii) the half-peak widths of the initial Ni powder. Accordingly, four calculations for each investigated powder were performed.

The milled Ni/8YSZ powder mixtures as well as the initial pure Ni powder were uniaxially pressed into specimens of 20 mm length, 5 mm width and 4 mm

height, applying a pressure of 610 MPa for the Ni/8YSZ mixtures and 210 MPa for the Ni powder. Solutions of polyvinylacetate in acetone (20%) for the former and polyvinylalcohol in ethanol (5%) for the latter were used as adhesion aids. The green samples were sintered in argon with 4 vol % of hydrogen (120 K h^{-1} heating, 300 K h^{-1} cooling). After sintering, the samples were annealed in the same atmosphere at 1000 °C for up to 1000 h. The relative density of the green, sintered and annealed samples was determined by calculating the density from the sample's weight and volume and dividing it by the theoretical density of the powder composition. The development of the pore structure of two Ni/10 vol % 8YSZ samples, one in the sintered state and one after annealing, were measured in more detail by mercury porosimetry (Pascal 140 and 440, Fisons Instruments, Italy). In the sintered state and after 100, 280 and 1000 h of annealing, the specific electrical conductivity of the samples was measured at 20 °C to determine structural changes. A four-point d.c. technique with the four copper electrodes placed in one line was used. The outer two electrodes were the current carrying electrodes, and the two inner electrodes (placed 10 mm apart) were used as voltage probes. Direct current ranging from 150 mA up to 4 A was applied. The samples were not affected by the conductivity measurement, making it possible to measure the same sample after various annealing times. The microstructure of samples in the sintered and 1000-h-annealed state were examined by optical metallography. Samples consisting of mechanically alloyed Ni with 10 vol % 8YSZ were also investigated by transmission electron microscopy (TEM) to observe the dispersoid structure and morphology.

3. Results and discussion

3.1. Powder characterization

The change of the mean particle size as a function of milling time is given in Fig. 1 for all produced powder batches. The pure Ni powder shows a strong initial particle coarsening, resulting from particle welding. The particle size increases from 6.4 μm up to more than 100 μm in the first hours of milling. With further increase of milling time the particle size decreases significantly. This results from embrittlement of the Ni leading to breaking down of the particles with further milling. In addition, further welding is hindered by the increasing proportion of the ceramic phase due to zirconia wear and Ni oxidation. By increasing the proportion of 8YSZ in the Ni powder, the initial particle coarsening is systematically reduced. Again, these observations can be attributed to the hindrance of nickel welding by the ceramic particles. Comparing the change in particle size of the two Ni 25 vol % 8YSZ batches (MA3, MA5), one can see that the particle size approaches a limiting value. Although batch MA5 was milled at higher energy (250 r.p.m.) than batch MA3 (150 r.p.m.), both batches show only a slight difference in particle size of less than 25% after milling for 90 h. All milled powder batches showed an almost ideal Gaussian distribution of their

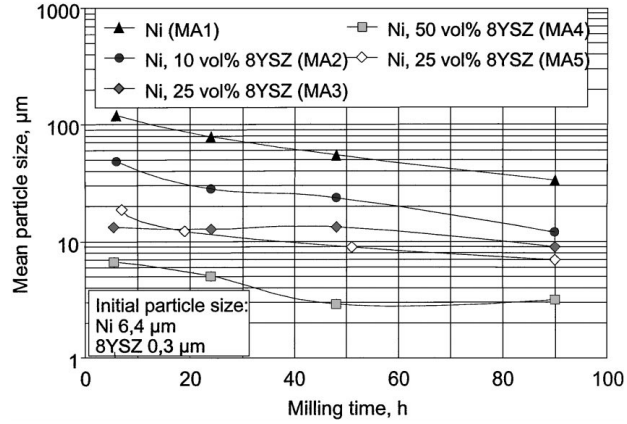

Figure 1 Decrease in particle size with milling time.

particle sizes, indicating that the fine particles of the broken 8YSZ agglomerates were dispersed in the Ni particles or at least stuck to them.

The X-ray diffraction patterns of all prepared powder batches after 90 h of milling are shown in Fig. 2. Only peaks related to Ni or 8YSZ can be seen. The NiO formed during milling could not be detected, which is because of its low proportion of approximately 4 wt %. The broadening of the Ni peaks with increasing amount of 8YSZ as well as with higher energy milling is clearly visible. The half-widths of the most intensive Ni peak have been determined, and the results are in good agreement with the above mentioned observations, see Table II. After a heat treatment at 900 °C for one hour the half-peak width decreased to that of the initial Ni powder. Peak broadening is mainly caused by an increasing number of defects like vacancies and dislocations as well as from grain refinement with increasing introduced milling energy and 8YSZ amount. During the short heat treatment, the defect density decreased and grain growth set in, leading to a decrease of the half-peak width. Two batches with 25 vol % of 8YSZ were analyzed in more detail by measuring at 2Θ angles up to 150 °. Consequently, 5 Ni peaks could be analyzed, and the result for lattice

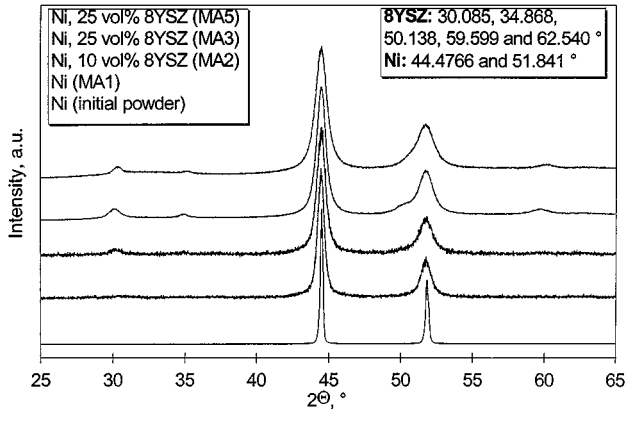

Figure 2 X-ray diffraction patterns of all prepared powder batches (listed from top to bottom); additionally the peak locations of 8YSZ and Ni are listed.

TABLE II Half-peak widths $\Delta 2\Theta$ of the most intensive Ni peak in the X-ray diffraction patterns of Fig. 2

Batch	2Θ (deg)	$\Delta 2\Theta$ (deg)
Ni, initial powder	44.4766	0.1508
Ni (MA1)[a]	44.4104	0.5259
Ni, 10 vol % 8YSZ (MA2)[a]	44.4100	0.6982
Ni, 25 vol % 8YSZ (MA3)[a]	44.4036	0.7319
Ni, 25 vol % 8YSZ (MA5)[b]	44.3938	0.9319
Ni, 25 vol % 8YSZ (MA3)[a], annealed at 900 °C/1 h	44.455	0.159

[a]Milled for 90 h at 150 r.p.m.
[b]Milled for 90 h at 250 r.p.m.

TABLE III Mean crystallite size and apparent lattice distortion for two [Ni/25 vol % 8YSZ] powder batches after 90 h of milling (1 corrected with a constant value of 0.13 °, 2 corrected with $\Delta 2\Theta$ of the initial Ni powder) [8]

Batch	Mean crystallite size (nm)	Apparent lattice distortion (%)	Correction method for $\Delta 2\Theta$	Assumed peak shape
MA3	24	0.86	1	Gauss
(150 r.p.m.)	36	0.86	1	Cauchy
	23	0.87	2	Gauss
	43	0.96	2	Cauchy
MA5	12	0.69	1	Gauss
(250 r.p.m.)	16	0.69	1	Cauchy
	13	0.69	2	Gauss
	17	0.8	2	Cauchy

distortion and crystallite size are given in Table III. The lattice distortion of the nickel changed only slightly with higher energy milling achieved by a higher rotation speed of the mill container. Both powder batches were extremely fine-crystalline, resulting from the formation of subgrain structures due to high energy milling. The crystallite size was substantially reduced by the higher milling energy at 250 r.p.m.

The peak broadening is correlated with a peak shift for both phases, see Figs 3 and 4. This shift results from the change in lattice constants given in Table IV. It should be pointed out that due to the relatively small effects compared to the scatter of the data this conclusion is somewhat tentative. Solution of the larger zirconium atoms ($r = 0.157$ nm) in the nickel lattice ($r = 0.124$ nm) can cause a slight expansion of the nickel lattice [8]. Under equilibrium conditions up to 1 at % of zirconium can be dissolved in Ni [9]. The more significant contraction of the 8YSZ lattice in sample MA5 is probably a consequence of Ni^{2+} solution in 8YSZ. After annealing at 1600 °C and rapid cooling down to room temperature, an amount of 3 mol % NiO was dissolved in 5YSZ (5 mol % Y_2O_3-stabilized zirconia), and of 10 mol % in 10YSZ [10, 11]. The change in lattice constant of Ni can be reversed by a short heat treatment (900 °C, 1 h), indicating that a fast precipitation process in Ni takes place during the short heat treatment.

The discussed changes in the structure of the milled Ni/8YSZ powder mixtures demonstrate that the high energy milling process was suitable for establishing the desired microstructure in the powder mixtures.

TABLE IV Change in lattice constants of Ni and 8YSZ due to high-energy milling

Batch	a_{Ni} (nm)	a_{8YSZ} (nm)
Ni or 8YSZ (initial material)	0.35242 ± 0.0009[a]	0.5139[a]
Ni, 25 vol % 8YSZ (MA3, 150 r.p.m.)	0.35268 ± 0.0043	0.51384 ± 0.00096[b]
Ni, 25 vol % 8YSZ (MA5, 250 r.p.m.)	0.35291 ± 0.000043	0.5109 ± 0.00095[b]
Ni, 25 vol % 8YSZ (MA3, 150 r.p.m.), annealed at 900 °C/1 h	0.35254 ± 0.00009^2	0.51296 ± 0.00032[b]

[a]JCPDS-ICDD 30-1468 $Y_{0.15}Zr_{0.85}O_{1.93}$.
[b]Values give the tendency, but may be inaccurate due to the small peak sizes.

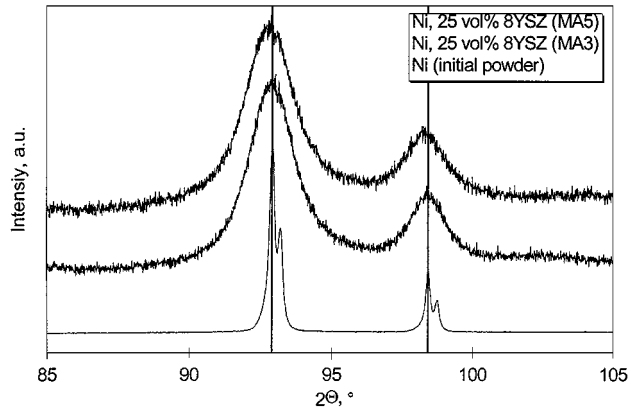

Figure 3 Displacement of the Ni peaks at 92.9103 ° and 98.4184 ° (listed from top to bottom).

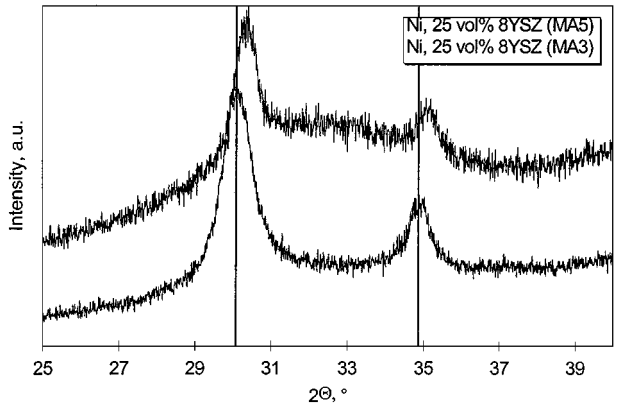

Figure 4 Displacement of the 8YSZ peaks at 30.085 ° and 34.868 ° (listed from top to bottom).

3.2. Sintering behavior

The sintering behavior of samples made up of the initial Ni powder as well as of milled Ni/8YSZ powder mixtures is shown in Fig. 5. Under the same sintering conditions, the Ni samples densify much more than all other samples. This is somewhat surprising because they had the lowest green density (see Fig. 5), and they

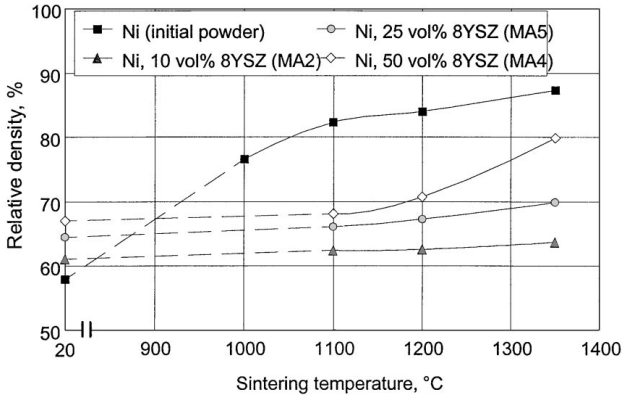

Figure 5 Sintering behavior of pressed nickel samples with various 8YSZ amounts (sintering time 1 h, at 1350 °C/2 h, atmosphere Ar/4% H_2).

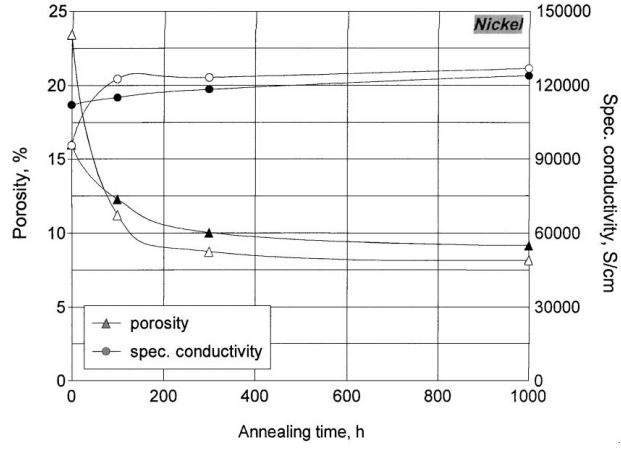

Figure 6 Changes of porosity and electrical conductivity with annealing time at 1000 °C in Ar/4% H_2 for Ni samples (i) sintered at 1000 °C (open symbols) (ii) sintered at 1200 °C (closed symbols).

were made of unmilled and therefore coarse-grained powder. In contrast, the relative density of the mechanically alloyed Ni 10 vol % 8YSZ samples increases only slightly with increasing sintering temperature. Even sintering at 1350 °C, which is approximately 100 °C below the melting point of Ni, causes only a slight densification compared to the sample's green density. This provides a first clue that sintering processes in Ni are strongly influenced by the amount of dispersed 8YSZ. The mechanically alloyed samples containing 25 and 50 vol % of 8YSZ show also a slight densification after sintering at 1100 °C. However, their densification increases systematically at higher sintering temperatures, and this effect is intensified by a higher amount of 8YSZ. We believe that this is an effect of 8YSZ sintering at temperatures high enough to enable sintering processes in 8YSZ. This is possible by two mechanisms:

(i) For the samples made of these powder mixtures the 8YSZ amount is only partially dispersed in the nickel particles, as observed by optical metallography. Accordingly, the observed densification may result from sintering of the agglomerated (not dispersed) 8YSZ,

(ii) If the amount of dispersed 8YSZ in the Ni matrix exceeds a critical amount, the so-called percolation point, the zirconia will start to build a connected network. In a system consisting of two spherical phases of equal size, for example, the percolation point amounts to 16 vol % [12]. We assume that the amount of dispersed 8YSZ in the samples containing 25 and 50 vol % of 8YSZ exceeds the percolation point. Hence, it follows that a densification of the composite can occur by sintering of 8YSZ particles.

Changes in porosity and electrical conductivity as a function of annealing time at 1000 °C can be seen in Figs 6 to 9 for samples with various 8YSZ amounts. The porosity of the Ni samples (Fig. 6) decreases significantly in the first hours of annealing, and approximates afterwards to a limiting value. The increase of the specific conductivity with annealing time correlates with the decrease of porosity. By optical metallography of the microstructure, a transition with annealing time from open porosity and elongated pores to closed porosity and isolated, spherical pores was observed. Accordingly, a final sintering state was reached. For a

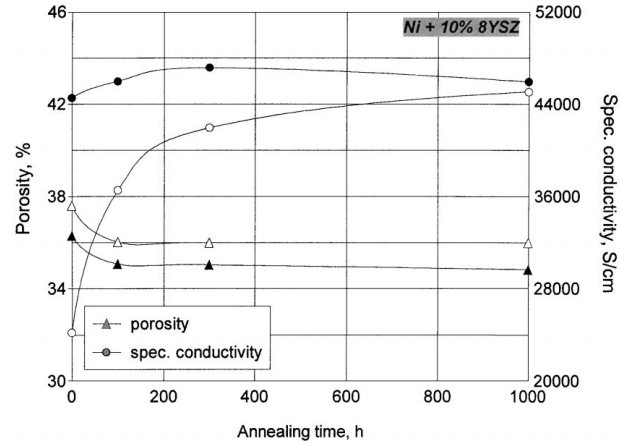

Figure 7 Changes of porosity and electrical conductivity with annealing time at 1000 °C in Ar/4% H_2 for Ni 10 vol % 8YSZ samples (i) sintered at 1100 °C (open symbols) (ii) sintered at 1350 °C (closed symbols).

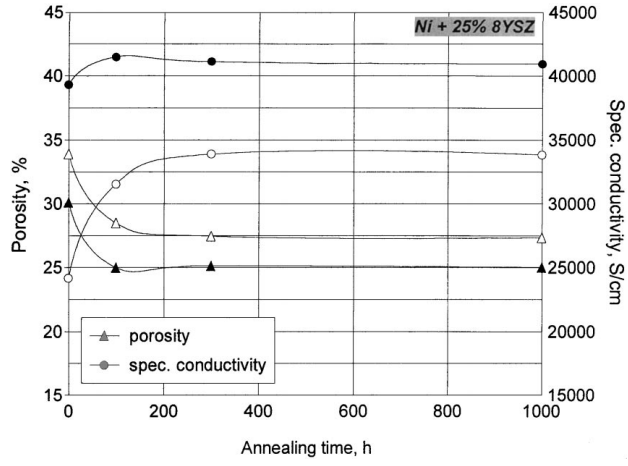

Figure 8 Changes of porosity and electrical conductivity with annealing time at 1000 °C in Ar/4% H_2 for Ni 25 vol % 8YSZ samples (i) sintered at 1100 °C (open symbols) (ii) sintered at 1350 °C (closed symbols).

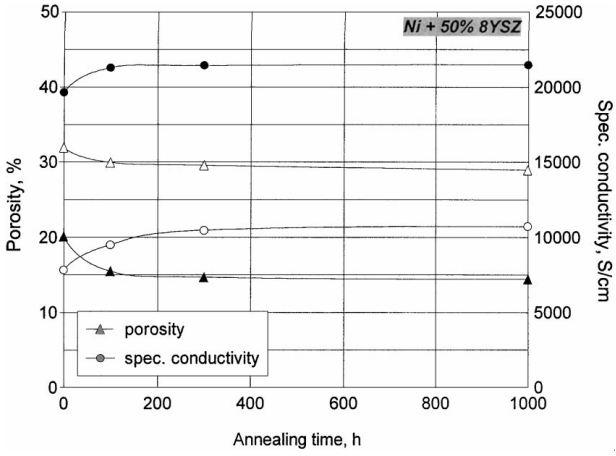

Figure 9 Changes of porosity and electrical conductivity with annealing time at 1000 °C in Ar/4% H_2 for Ni 50 vol % 8YS samples (i) sintered at 1100 °C (open symbols) (ii) sintered at 1350 °C (closed symbols).

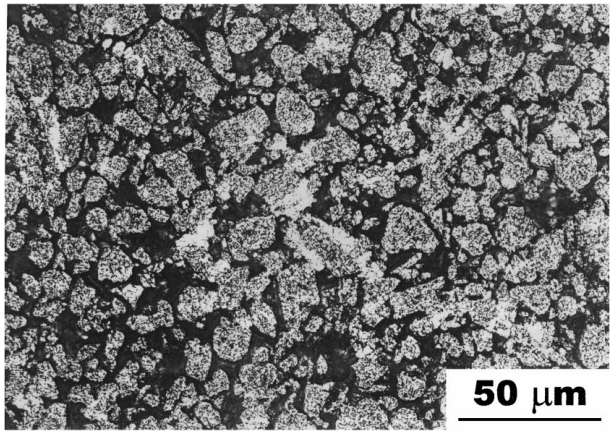

Figure 10 Optical micrograph of an etched [Ni/10 vol % 8YSZ] sample, sintered at 1100 °C, before annealing.

specimen, sintered at 1000 °C, the grain size of nickel increased from approximately 10 μm up to 90 μm during annealing. These microstructural changes demonstrate that a "complete annealing" (also termed "soft annealing") occurred, during which recrystallization with subsequent grain growth took place. For Ni, a temperature of 700 °C or more is required for this heat treatment [13]. In agreement with the microstructural changes, the specific conductivity reaches nearly the theoretical value of pure, dense Ni (137 000–147 000 S cm^{-1}, [13]) during annealing.

In contrast, the Ni samples alloyed with 10 vol % of 8YSZ show only a slight porosity decrease in the first 100 h of annealing, see Fig. 7. With further annealing, the amount of porosity does not decrease further. Although the amount of porosity is nearly constant, the pore morphology changes clearly after annealing at 1000 °C, see Figs 10 and 11. Before annealing, the pore structure is wide open, and the pores are elongated. The Ni particles are connected by small necks. After annealing, the particles are so connected that initial particles and necks are hardly distinguishable. The pores exhibit a more spherical shape, but the porosity is still open. This correlates with a transition from an early to an intermediate state of sintering.

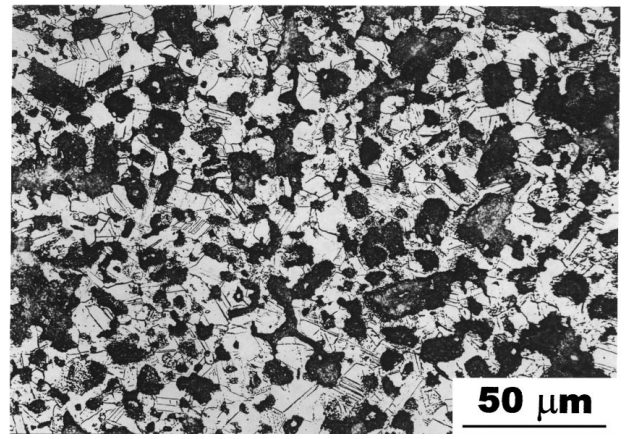

Figure 11 Optical micrograph of an etched [Ni/10 vol % 8YSZ] sample, sintered at 1100 °C, after annealing (1000 °C, 1000 h).

An even more significant change occurred in the grain structure of the Ni phase. Before annealing, an extremely fine-grained Ni structure could be seen, which was in good agreement with the results from the structural analysis by X-ray diffraction. After annealing, the Ni grains were coarsened. A large number of twin crystals could be seen, which is typical for recrystallized Ni. Obviously, recrystallization and grain growth occurred. However, these processes did not lead to an excessive grain growth as observed in pure Ni. Only slight particle growth and densification was observed. Accordingly, the recrystallization was strongly inhibited. This results from the reduction of grain boundary mobility by the dispersions and the observed low density, which is due to the retardation of the sintering processes in Ni by the dispersoids. For TD nickel (nickel with 2 vol % dispersion of fine thoria particles), a retardation of recrystallization has been reported in the literature, leading to an increase of the recrystallization temperature compared to that of pure nickel [14]. The solution of zirconium in the Ni matrix may cause an effect additional to the recrystallization retardation: an additon of 0.1 wt % zirconium causes approximately a 400 °C rise in recrystallization temperature above that of pure nickel [14].

The pore size distribution before and after annealing is given in Fig. 12 for Ni 10 vol % 8YSZ samples sintered at 1100 °C. Mercury porosimetry was used,

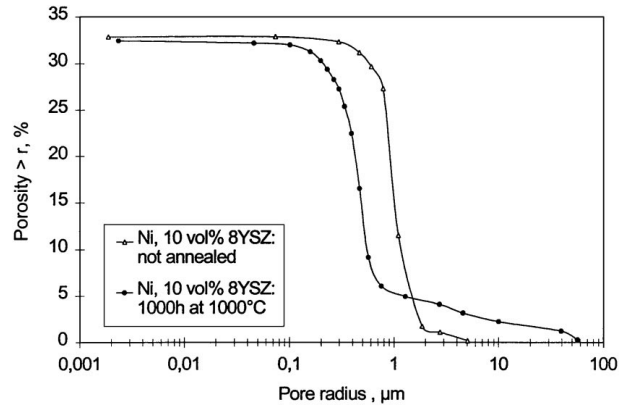

Figure 12 Pore size distribution for Ni 10 vol % 8YSZ, sintered at 1100 °C, before and after annealing (1000 °C, 1000 h).

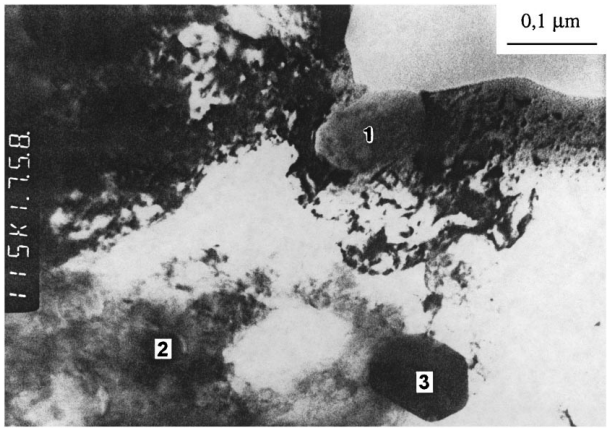

Figure 13 TEM showing dispersoid morphology in Ni 10 vol % 8YSZ after sintering at 1350 °C and annealing at 1000 °C for 1000 h; section near the Ni particle surface, three 8YSZ particles are indicated.

and hence only open porosity could be evaluated. Accordingly, the measured total porosity was lower than the geometrically obtained porosity (Fig. 7). The total porosity decreased slightly from 32.9% in the sintered state to 32.4% after annealing, but the mean pore radius decreased from 1 μm to 0.5 μm. In addition, the number of pores larger than 1 μm in radius substantially increased after annealing, resulting in a broadening of the pore size distribution. These observations demonstrate that sintering processes occurred, whereby large pores grew at the expense of small pores, e.g. by surface diffusion. However, no significant particle center approach, leading to a densification of the sample, took place.

The dispersoid which was added by an amount of 10 vol % cannot be detected in the photomicrographs of Figs 10 and 11. To prove the dispersoid structure, one [Ni/10 vol % 8YSZ] sample was observed by TEM. The sample was sintered at 1350 °C and annealed at 1000 °C for 1000 h. A rather homogeneous distribution of dispersoids with sizes ranging from 20 to 100 nm was detected. Their size is almost in the same range as that of the 8YSZ crystallites in the initial 8YSZ powder. Hence it follows that the initial 8YSZ powder particles were deagglomerated and crushed during the high-energy milling process, and that the remaining small crystallites were finally dispersed in the Ni particles. Fig. 13 shows a section of a Ni particle including three (numbered) 8YSZ dispersoids. An amount of 45 at % Zr, 51 at % Ni and 4 at % Y was measured by energy dispersive spectroscopy (EDX) at spot 1 showing a 8YSZ particle in the nickel matrix.

The results presented here clearly indicate that the observed dispersion of nano-sized 8YSZ crystallites in the Ni matrix inhibit the sintering of the Ni particles. Ashby *et al*. [6] discussed several mechanisms which can be responsible for this effect. They pointed out that the phenomena can be understood in terms of a threshold potential which is introduced by the dispersed particles. These threshold potentials lower the gradient in the chemical potential and lead thereby to a reduction of the sintering rate. The magnitude of the so-called surface threshold can be estimated by calculating the energy necessary to isolate the particle. Under the assumption that the particle-free surface energy is equal to the free energy of the particle–matrix interface (i.e. partly wetting dispersoids) the threshold potential is equal to:

$$\Delta\mu_i^s = \frac{3f\Omega\gamma_s}{d} \tag{1}$$

where f is the volume fraction of the dispersed particles, Ω the atomic volume, γ_s the free surface energy of the powder, and d the diameter of the dispersed particles.

We now derive a crude estimate of the conditions under which a significant influence of the dispersed particles on sintering is expected. A similar estimate is given in [6]. The threshold energy will have a significant effect if it is comparable to the difference in chemical potential which drives diffusion:

$$\mu_s = \frac{2\gamma\,\Omega}{r} \tag{2}$$

where r is the particle diameter. Hence, if the ratio

$$\frac{\Delta\mu_i^s}{\mu_s} = \frac{3fr}{2d} \tag{3}$$

is comparable to or larger than one, a significant effect is expected. For the 10 vol % samples we can calculate this ratio to be about 30. The strong inhibition of densification (Fig. 5) as well as the minor microstructural changes during annealing (Fig. 7) correspond to the result of this estimate.

The specific conductivity of the Ni phase in the samples alloyed with 10 vol % 8YSZ, estimated by the rule of mixtures regarding the pore and 8YSZ volumes, amounts to approximately 83 000 S cm^{-1} after annealing. This is only 59% of the theoretical conductivity of Ni. It is assumed that the substantially reduced conductivity values results from the higher density of defects in the annealed Ni with 10 vol % 8YSZ compared to the pure Ni. These defects are dislocations, which are pinned at the dispersoids, the small dispersoids themselves (the finest might have sizes of the order of the mean free path of the electrons) and grain boundaries, which are present in a higher volume fraction due to the finer grain size.

The samples containing Ni with 25 and 50 vol % of 8YSZ showed a significant decrease of their porosity in the first hours of annealing, see Figs 8 and 9. The decrease amounted to 3–6% and was higher than that of the samples containing 10 vol % of 8YSZ. It coincided with an increasing specific conductivity, whereby this increase was lower when the samples had been sintered at higher temperature. Accordingly, the recovery processes which caused the increasing conductivity had already occurred during sintering for the higher sintered samples. In the microstructure of these samples, see Figs 14 and 15, several phases have been detected: (i) a light and homogeneous phase, which consists of Ni with an unknown amount of dispersoids, (ii) a gray, inhomogeneous phase consisting of Ni and 8YSZ particles, and (iii) pure 8YSZ, which exists only in the samples with 50 vol % of 8YSZ. It is evident that the zirconia is

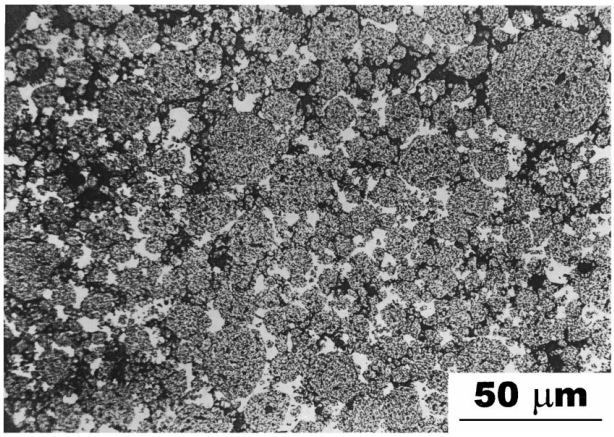

Figure 14 Optical micrograph of Ni 25 vol % 8YSZ, sintered at 1100 °C, before annealing.

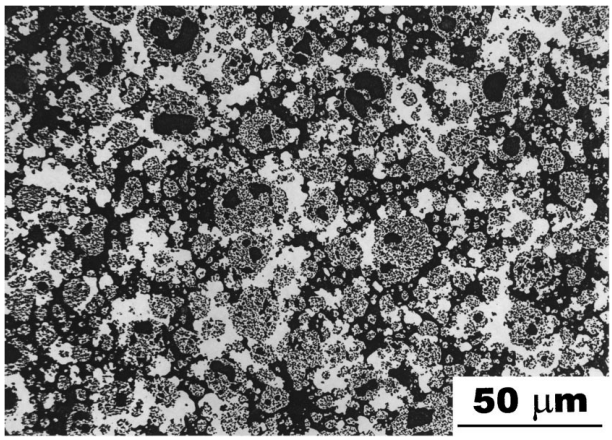

Figure 15 Optical micrograph of Ni 25 vol % 8YSZ, sintered at 1100 °C, after annealing.

distributed inhomogeneously in the samples. The presence of the Ni phase indicates that with higher zirconia content the dispersion of the 8YSZ into all Ni particles becomes increasingly difficult. After annealing, the amount of the light phase increased, and the structure of the inhomogeneous phase coarsened. As mentioned above, we assume that these changes result from sintering of the un-dispersed 8YSZ on the one hand, leading to a coarsening of the zirconia in the inhomogeneous phase. On the other hand, the retardation of Ni sintering will be reduced in the Ni with the high proportion of 8YSZ because a large fraction of the Ni particles do not contain sufficient amounts of dispersoids. A coarsening of the rather pure Ni phase will occur and, consequently, the amount of the light phase will increase. Similar results have also been found in Ni and Co powders with MgO and CaO dispersions [15]. A minimum densification rate was reached at about 7–10 vol %; at higher volume fractions the rate increased slightly, probably due to agglomeration.

4. Conclusions

The applied mechanical alloying of the Ni/8YSZ powder mixtures by dry ball milling was suitable for producing extremely fine-grained powder particles with a homogeneous particle size distribution. Structural changes like lattice distortion and grain refinement of Ni and shifting of the lattice constants of Ni and 8YSZ were observed after high-energy milling. The 8YSZ particles were dispersed in the Ni particles or at least stuck to their surfaces. Samples made of mechanically alloyed Ni with 10 vol % 8YSZ showed a retardation of recrystallization and a significantly lowered densification during sintering at temperatures up to 1350 °C as well as during annealing at 1000 °C, compared to samples made of the initial Ni powder. Even after 1000 h at 1000 °C, they are less densified than pure Ni samples after only 1 h at 1000 °C. This results from a homogeneous dispersion of 8YSZ crystallites in the Ni matrix, which was observed by TEM. The dispersoid structure obviously hinders sintering processes. The attempt to produce a suitable anode substrate for a SOFC by high-energy milling of Ni with 25 or 50 vol % of 8YSZ, respectively, pressing and finally sintering of the green substrate was not successful: these samples showed a higher densification during sintering and annealing than samples containing 10 vol % 8YSZ. We assume that this higher densification results from sintering of the un-dispersed agglomerated 8YSZ, which was inhomogeneously distributed in the samples, as well as from sintering of the dispersed 8YSZ in the Ni matrix as a consequence of exceeding a critical 8YSZ proportion (percolation point).

Mechanically alloyed nickel, which exhibits a homogeneous dispersion of 8YSZ crystallites in the Ni matrix, is a promising candidate for the catalytic material of a SOFC anode or for general application as a high-temperature catalyst. Under SOFC working conditions, the degradation of the anode's performance due to Ni sintering can be substantially diminished by the dispersoid structure, and accordingly the long-term stability of the whole SOFC system is enhanced.

Acknowledgements

We are indebted to P. Lersch and H. Hoven (Institut für Werkstoffe und Verfahren der Energietechnik, Forschungszentrum Juelich GmbH) and Dr B. Sktrotzki (Institut für Werkstoffe, Ruhr-Universität Bochum) for valuable experimental work.

References

1. N. Q. MINH, *J. Am. Ceram. Soc.* **76** (1993) 563.
2. W. SCHAEFER et al., in Fourteenth Risoe International Symposium on Materials Science Proceedings Roskilde, 6–10 September 1993, edited by F. W. Poulsen (Risoe National Laboratory, 1993) pp. 409–416.
3. R. WILKENHOENER, TH. KLOIDT and W. MALLENER, in Electrochemical Proceedings Vol. 97-40, edited by U. Stimming et al. (The Electrochemical Society, Inc., Pennigton, New Jersey, 1997) pp. 851–860.
4. R. C. BENN and P. K. MIRCHANDANI, in "New Materials by Mechanical Alloying Techniques" (DGM Informationsgesellschaft Verlag, Oberursel, 1989) pp. 19–38.
5. G. C. KUCZYNSKI and H. W. LAVENDEL, *Int. J. Powder Metall.* **5** (1969) 19.
6. M. F. ASHBY, S. BAHK, J. BEVK and D. TURNBULL, *Prog. Mater. Sci.* **25** (1980) 1.
7. H. LIPSON and H. STEEPLE, in "Interpretation of X-Ray Powder Diffraction Patterns" (Macmillan, London, 1970).

8. E. FLUCK, in "Allgemeine und Anorganische Chemie" (Quelle und Meyer, Heidelberg, 1984).
9. in "Phase Diagrams of Binary Nickelalloys," edited by P. Nash (ASM International, Ohio, 1991).
10. S. CHEN, *Mater. Sci. Eng. A* **158** (1992) 251.
11. *Idem*. *Mater. Sci. Eng. B* **22** (1994) 247.
12. H. SCHER and R. ZALLEN, *J. Chem. Phys.* **53** (1970) 759.
13. R. J. MEYER and E. H. E. PIETSCH, in "Gmelins Handbuch der anorganischen Chemie (Nickel, Teil AII-Lieferung 1)" (Verlag Chemie GmbH, Weinheim/Bergstr., 1967) p. 199 and p. 353.
14. S. ROSENBERG, in "Nickel and Its Alloys," NBS Monograph 106 (U.S. Department of Commerce, National Bureau of Standards, United States Government Printing Office, Washington, 1968) p. 18.
15. M. H. TIKKANEN, B. O. ROSELL and O. WIBERG, *Powder Metall.* **10** (1962) 49.

Received 1 June
and accepted 18 August 1998